Radiation damage evaluation of materials for radiotherapy quality assurance devices under high dose and ultra-high dose rate electron and proton beams

M. Orts [1,], Y. C. Gedik [2,3], A. Bourgouin [2,4], Ralf-Peter Kapsch [2], C. Koumeir [5,6], T. Sounalet [6], S. Rossomme [7], K. Souris [7] and E. Sterpin [1,8,9].*

[1] UCLouvain, Institut de Recherche Expérimentale et Clinique, Molecular Imaging Radiotherapy and Oncology (MIRO), Brussels, Belgium.
[2] Dosimetry for Radiation Therapy and Diagnostic Radiology, Physikalisch-Technische Bundesanstalt (PTB), Braunschweig, Germany
[3] Nuclear Energy Research Institute (NÜKEN), Turkish Energy Nuclear and Mineral Research Agency (TENMAK), Ankara, Turkey
[4] Metrology Research Center, National Research Council of Canada (NRC), 1200 Montreal Road, Ottawa, ON, K1A0R6, Canada)
[5] GIP ARRONAX, Saint-Herblain, France
[6] Laboratoire SUBATECH, IMT Atlantique CNRS-Université de Nantes, Nantes, France
[7] Ion Beams Applications S.A., Dosimetry Business Unit, Louvain La Neuve, Belgium
[8] KU Leuven, Department of Oncology, Laboratory of Experimental Radiotherapy, Leuven, Belgium
[9] Particle Therapy Interuniversity Center Leuven, Particle, Leuven, Belgium
[*] *Author to whom any correspondence should be addressed.* *E-mail : marina.orts@uclouvain.be*

1. Abstract

Motivation: FLASH radiotherapy is a promising technique based on the delivery of ultra-high dose rates (UHDR) to spare healthy tissue. Robust quality assurance (QA) is required to ensure a safe delivery of the treatment. QA devices such as phantoms and ionization chambers are typically made out of polymeric materials to ensure water equivalence. However, radiation exposure, particularly at UHDR where achieving high doses is easier, may cause irreversible changes to the structure of these materials. These extreme conditions can compromise the integrity and reliability of QA devices.

Objectives: This study aims to characterize radiation damage in common materials used for QA devices and identify which of them can withstand these challenging conditions.

Materials and methods: A variety of materials commonly used in phantoms and ionization chambers, with diverse characteristics (transparent, opaque, conductive and non-conductive) were irradiated using 68 MeV proton and 20 MeV electron beams, reaching doses up to 1 MGy under UHDR conditions (average dose rates of 100 – 500 Gy/s). Material damage was evaluated through optical, chemical, mechanical and electrical tests to quantify change in color, structural integrity, and relevant electrical properties such as conductivity and dielectric constant that can affect detector response.

Results: External appearance of some materials significantly changed after irradiation. All transparent materials exhibited change in color post-irradiation. Chemical analyses conducted after irradiation and repeated two years later indicated partial recovery in some materials. No significant difference in damage was observed between proton and electron irradiation, suggesting comparable radiation damage mechanisms. Dose rate alone did not exacerbate damage beyond total dose effects; however, extended irradiation at high dose rates resulted in thermal damage under some conditions. Mechanical testing revealed increased fragility, changes in hardness and dimensions, while some materials experienced significant changes in dielectric constant and conductivity.

Conclusion: Materials such as PMMA, PC, POM, and its conductive variant POM ELS, are unsuitable for prolonged irradiations at UHDR due to significant structural degradation observed. For see-through phantom construction, CPS offers a more durable alternative to PMMA. For detector construction, PEEK (for non-conductive parts) and graphite (for conductive parts) demonstrated promising durability, making them preferable choices under high dose and UHDR conditions. The higher stability of these materials can be attributed to the presence of aromatic rings in their chemical structure, which enhances radiation resistance.

1. Introduction

Polymeric materials are widely employed in the field of radiation therapy, particularly in the construction of quality assurance (QA) devices such as ionization chambers (ICs), water tanks, and phantoms. These materials are preferred due to their unique properties, including mechanical strength, radiation resistance, and water equivalence – a key property for accurate dose measurements, as emphasized by the International Atomic Energy Agency (IAEA) protocol TRS-398 (Andreo et al., 2024).

FLASH radiotherapy, an emerging cancer treatment modality, delivers therapeutic doses at ultra-high dose rates (UHDR), several orders of magnitude higher than those used in conventional radiotherapy ($\gtrsim$ 40 Gy/s (Zhou et al., 2020)). This promising technique has demonstrated to spare healthy tissues while effectively controlling tumors (Favaudon et al., 2014) and has been observed with different particles (Diffenderfer et al., 2020; Montay-Gruel et al., 2019). Particularly for QA devices, among other challenges (Martino et al., 2020; Subiel et al., 2024), high doses are easily achieved in a short time, accelerating the material degradation. When polymeric materials are irradiated, they undergo complex chemical and physical processes, including macromolecular chain scission, cross-linking, and free-radical formation (Ferry et al., 2016). Over time, these processes result in cumulative defects that may degrade the material's properties. This degradation may be particularly pronounced under UHDR conditions, as illustrated in *Figure 1*, where significant degradation of commercially available ICs and water phantoms exposed to UHDR is shown.

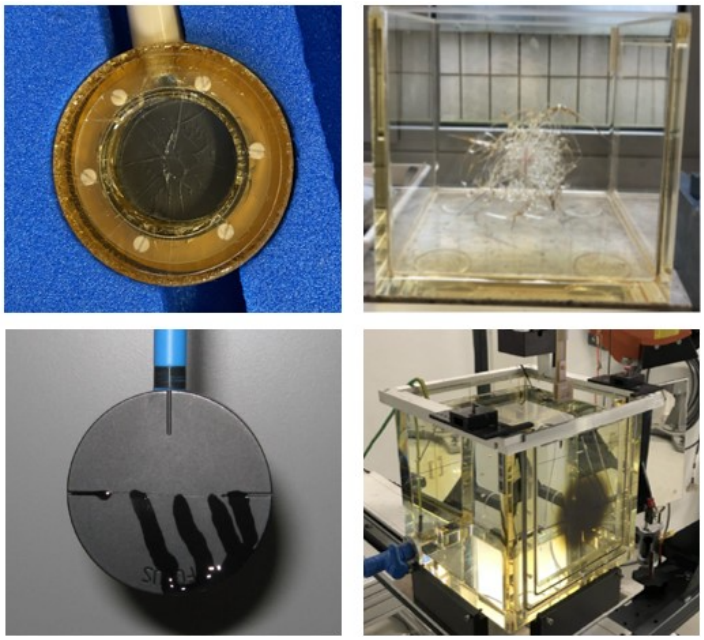

Figure 1: Commercial ICs and water phantoms after exposure to very high dose and ultra-high dose rates.

The functional requirements of QA materials vary depending on their application. Transparency is essential for devices such as water tanks and phantoms, where precise alignment with positioning laser systems is critical. In contrast, materials used in ICs do not require optical clarity. But they require durability and a combination of conductive and non-conductive components. These differing characteristics require the selection of polymers tailored to their specific applications. Given the importance of QA devices in ensuring the safe delivery of radiotherapy, it is vital to understand the limits of radiation-induced degradation of materials used in their construction.

This study aims to evaluate the structural and functional changes in commonly used materials for QA device construction under UHDR conditions. Specifically, it investigates how particle type – in this study specifically electrons and protons – total dose deposited and dose rate influence material degradation. By establishing the tolerances of these materials and identifying the most resistant materials to UHDR exposure, this work aims to provide recommendations for the selection of durable materials for QA device construction suited for UHDR radiotherapy applications.

2. Materials and methods

2.1. Materials

Two different sets of samples focused for different applications were used for this study, with their characteristics summarized in Table 1. Figure 2 provides an illustration of the two kinds of samples. The first set, referred to as *Type "E",* is intended for studying thicker materials typically used in the manufacturing of water tanks and phantoms. The geometry selected is a rectangular prism of 10 x10 mm^2 surface with the following materials and thicknesses: 3 mm, 5 mm, 10 mm, 15 mm and 20 mm Polymethyl Methacrylate (PMMA); 5 mm and 20 mm Polyether ether ketone (PEEK); 5 mm Polycarbonate (PC); 5 mm Cyclic Olefin Copolymer (TOPAS) and 4.8 mm Clear Polystyrene (CPS).

The second set of samples, labeled *Type "P",* focuses on studying thinner samples commonly used in the construction of ICs. While large recombination effects suggest that some ICs might not be suitable for UHDR electron beams (Bourgouin et al., 2023), the dose rates achieved with protons are not as high (Subiel et al., 2024), allowing ICs with smaller electrode spacing to be used under these circumstances even though recombination effects are still present (Subiel & Romano, 2023). Therefore, this set of samples was irradiated under proton beams. As recommended by international dosimetry protocols (Almond et al., 1999; Andreo et al., 2024), ICs with plane parallel geometry is preferred. Therefore, the chosen geometry is a disc with 2 mm inner diameter and 12 mm outer diameter with thickness of 0.5 mm, 1 mm, 1.5 mm and 2 mm. These dimensions are typical for ICs critical structures, such as the entrance window and collecting electrodes. The following materials are used for this set of samples: PMMA; PEEK; cross-linked polystyrene copolymer (REXOLIT); Polyoxymethylene (POM); C-552 (or SCHONKA, air equivalent plastic); Graphite; Electrically Conductive Polyoxymethylene (POM ELS) and Electrically Conductive Polyether ether ketone (PEEK ELS).

Material	Colour	Conductive	Geometry	Thickness (mm)	Density (g/cm^3)
PMMA	Transparent	No	Type E	$3, 5, 10, 15, 20$	1.19
			Type P	$0.5, 1, 1.5, 2$	1.18
PEEK	Beige opaque	No	Type E	$5, 10, 20$	1.32
			Type P	$0.5, 1, 1.5, 2$	1.21
PC	Transparent	No	Type E	5	1.20
TOPAS	Transparent	No	Type E	5	1.01
CPS	Transparent	No	Type E	4.8	1.05
REXOLITE	Transparent	No	Type P	$0.5, 1, 1.5, 2$	1.05
POM	White	No	Type P	$0.5, 1, 1.5, 2$	1.41
C-552	Black	Yes	Type P	$0.5, 1, 1.5, 2$	1.76
GRAPHITE	Black	Yes	Type P	$0.5, 1, 1.5, 2$	2.26
POM ELS	Black	Yes	Type P	$0.5, 1, 1.5, 2$	1.41
PEEK ELS	Black	Yes	Type P	$0.5, 1, 1.5, 2$	1.36

Table 1: Materials and relevant characteristics of the samples used in this study.

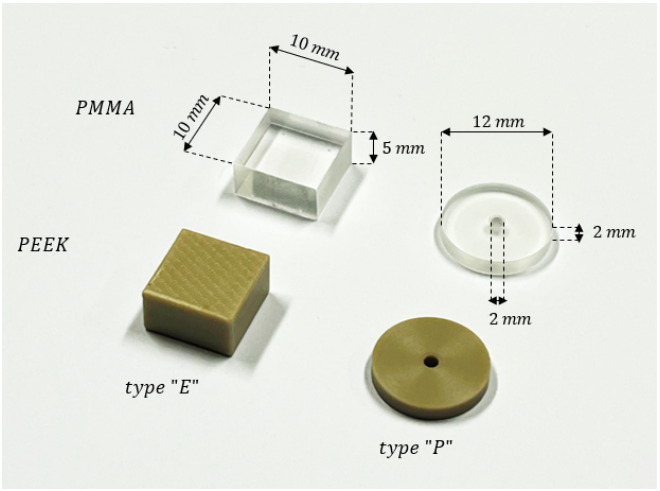

Figure 2: Example of Type "E" sample with a 10x10 mm^2 surface area and thickness of 5mm of PMMA and PEEK. Type "P" sample has an external diameter of 12mm, an internal diameter of 2mm and thickness of 2mm.

2.2. Experimental setup for irradiations

Type "E" samples were irradiated with a 20 MeV electron beam, at a 10 Hz pulse repetition frequency and a pulse width of 2.5 μs, inside a water tank at a Source to Surface Distance (SSD) of 50 cm. This resulted in a dose per pulse rate of about 10.5 Gy at the half-value depth (R_{50})(Andreo et al., 2024) of 7.14 cm. All sets of samples were positioned in the plateau region of the Percentage Depth Dose (PDD), i.e., at a depth of around 1 cm, to ensure the most uniform dose deposition through the sample. Samples were irradiated with six different dose levels: 10^2Gy, 10^3 Gy, 10^4 Gy, 10^5Gy, $5 \cdot 10^5$Gy and 10^6Gy. One sample per condition was kept unirradiated. The electron irradiation was carried out with the dedicated research LINAC from the Metrological Electron Accelerator Facility (MELAF) at PTB, Germany (Bourgouin et al., 2022). These conditions are labeled as experiment SSD50. For comparison with other dose rates, an additional set of PMMA and PEEK samples were irradiated under two extra experiments: SSD70 and SSD50-C. Detailed characteristics of these experiments are provided in Table 2. The dose delivered to the samples was estimated using the in-beamline integrating current transformer (ICT), which was calibrated with a diamond detector (Kranzer et al., 2022) that had been previously calibrated against alanine dose

measurements in a separate investigation (Bourgouin et al., 2022). Due to the not need of such precision in the dose delivered the uncertainty in the dose estimation was large, around 5%.

Experiment	Particle / Energy	Collimator	FWHM at Z ref (mm)	Pulse duration (μs)	Pulse repetition frequency (Hz)	SSD (cm)	Z ref (mm)	Instantaneous dose rate (Gy/p)	Instantaneous dose rate (Gy/s)	Average Dose Rate (Gy/s)	Total Dose (MGy)
SSD70	20 MeV e	None	79.9	2.5	5	70	46.2	6.47	2.59e6	32.4	0 - 1
SSD50-C	20 MeV e	Ø=5cm	49.7	2.5	10	50	41.2	11.5	4.60e6	115	0 - 1
SSD50	20 MeV e	None	47.3	2.5	10	50	41.9	10.5	4.20e6	105	0 - 1

Table 2: Experiment specifications for the electron (e) irradiations.

Type "P" samples were irradiated in air with a 68 MeV broad pulsed proton beam with the pulsing chopper-based system of the Arronax C70XP cyclotron (Poirier et al., 2019) at Arronax, France. The different dose levels and dose rates achieved are summarized in table 3. To achieve the $4x4cm^2$ field size, the beam was spreaded with a 300 μm tungsten target placed in the beamline, which resulted in an effective energy to the samples about 64 MeV, and collimated with paraffin blocks. For the $1x1cm^2$ field size, no target or collimator were added. The estimation of the average dose delivered to the samples in this setup was done using films (Villoing et al., 2022) for the profiles as the beam was not homogeneous. To estimate the dose, a Faraday cup was used to measure the cumulated dose and cross-calibrated against an IC at low dose rates where recombination losses can be corrected (Christensen et al., 2020; Rossomme et al., 2017).

Experiment	Particle / Energy	Field size (cm^2)	Pulse duration (ms)	Pulse repetition time (ms)	Instantaneous dose rate (Gy/s)	Average Dose Rate (Gy/s)	Total Dose (MGy)	Total irradiation time (h)
P1	68 MeV p	4x4	0.05	1.8	9.0e3	141	0.42	0.8
P2	68 MeV p	4x4	1	21	2.1e3	105	1.02	2.7
P3	68 MeV p	1x1	1	41	8.4e3	216	1.09	1.4
P4	68 MeV p	1x1	1	5	2.6e3	500	1.00	0.6

Table 3: Experiment specifications for the proton (p) irradiations. P0 would be the pristine, non-irradiated, samples.

2.3. Sample characterization

Assessing changes in optical, mechanical, chemical, and electrical properties is crucial, as irradiation-induced alterations may not be visible through simple observation but can significantly impact the accuracy, calibration, and functionality of dosimetry devices. For instance, reduced optical transmittance can affect laser alignment in water phantoms, while microstructural defects observed on material surfaces can reveal the onset of a mechanical failure. Chemical analysis can reveal degradation mechanisms whereas mechanical properties evaluation can detect dimensional changes that may cause misalignments, invalidating critical parameters in ICs such as calibration coefficients, quality correction factors, and ultimately, dose determination. Evaluating fragility is also important, as increased brittleness can lead to crack formation, potentially leaving the device unusable. Changes in electrical properties are particularly crucial for ICs, as significant variations in the permeability of non-conductive components can increase leakage current, while alterations in conductive components can compromise calibration coefficients. The following subsections detail the methods used to evaluate these properties.

2.3.1.Optical properties

A *UV-VIS-NIR Spectrophotometer UV-3600 Plus from Shimadzu* was used to quantify color changes in the irradiated samples by measuring changes in transmittance relative to the non-irradiated samples. The

transmittance spectrum was recorded across wavelengths ranging from 200 to 800 nm, with a resolution of 0.5 nm. Spectra were normalized at the lowest wavelength, and values were compared at 420 nm (Monsores et al., 2019). To enhance the signal-to-noise ratio and improve the readings accuracy, two measurements modes were used based on transparency. For highly transparent samples, transmittance mode was used. For non-transparent samples, measurements were conducted in absorbance mode and latter converted to transmittance using known relations.

A detailed analysis of the surface morphology through scanning electron microscopy (SEM) was performed on conductive samples, as non-conductive materials can accumulate surface charge under electron beam exposure, causing image distortion and signal artifacts. In this study, no conductive coating was applied to non-conductive samples to avoid altering their surface, ensuring that long-term follow-up analyses could be performed without compromising the original material properties. A *JEOL JSM – 7100F Field Emission Scanning Electron Microscope* was used under ultra-high vacuum conditions, employing accelerating voltages of 2, 5 and 15 kV and magnifications of x20, x200, x900 and x1600.

2.3.2. Chemical properties

To investigate chemical and molecular changes in the sample structure, Fourier Transform Infrared (FTIR) spectroscopy was performed using a *Nicolet iN10 Infrared Microscope* equipped with a Mercury Cadmium Telluride in Attenuated Total Reflectance (ATR) mode. Spectra were measured across a range of 675–4000 cm^{-1} with a resolution of 2 cm^{-1}, averaging 64 scans per sample to ensure a high signal-to-noise ratio. Background spectra were acquired and subtracted from each measurement. Standard pressure was applied to samples during collection, and the detector was cooled with liquid nitrogen to enhance sensitivity. After acquisition, all spectra were baseline-corrected, normalized, and analyzed using *Omnic Spectra software from Thermo Fisher Scientific Inc.*

Due to the specific relevance of graphite in ionization chamber construction (e.g., for collecting electrodes or walls in cylindrical ICs) and its use in other detectors such as graphite calorimeters, additional characterization of graphite samples was performed using Raman spectroscopy as FTIR is not suitable for graphite characterization due to its highly ordered structure and lack of infrared-active functional groups (Friedel & Carlson, 1971). A *Reinshaw Qontor inVia* Raman microscope was employed. The Raman spectra were acquired using a 785 nm laser, with measurements taken at multiple points across the sample surface. Acquisition parameters included an exposure time of 15 seconds, laser power set to 10%, and a total of 3 accumulations, with a Raman shift range of 827–1896 cm^{-1}. Automatic baseline correction was applied to all spectra, and the intensity of the G and D bands was analyzed to detect structural changes in the graphite samples.

2.3.3.Mechanical properties

A *Palmer micrometer* with a 1 μm resolution was used to identify possible changes in dimensions of the different samples. Hardness was evaluated via micro-indentation with the *Micro indenter EMCO Durascan 70G5* equiped with a Vickers tip. A quasi-static load function with a peak force ranging 0.05 - 1 N was applied. A minimum of 10 indentations were performed through the surface. Fragility was evaluated indirectly by observing the presence or absence of rifts around the indentation marks left by the hardness tests.

2.3.4. Electrical properties

The conductivity and dielectric constant of the samples were measured using a *Novocontrol ALPHA High Resolution Impedance/Dielectric Analyzer*. Measurements were conducted at a fixed AC voltage of 1 V, across a frequency range of 10^3 - 10^7 Hz of the applied alternating current (AC) voltage signal. Since the measured values of ε are highly dependent on the conditions under which the measurements are performed, all samples were analyzed on the same day and measurements were repeated across several days. ε values for comparison were taken at 100 Hz to mitigate the effects of capacitance dependence at higher frequencies, as described by (Gross et al., 2007). The relative change in ε with respect to non-irradiated samples was used for comparative analysis.

3. Results

Figures 3 and 4 show the external appearance of the different samples irradiated with electrons and protons. For PMMA type "E" samples, the gradual change in color with increasing dose levels is clearly visible. It can also be observed that optical density recovers over time - two years post-irradiation (Y2), when compared to the appearance shortly after irradiation (Y0), which aligns with trends described in the literature (Clough et al., 1995).

In general, gradual color changes were observed for all transparent materials. Significant opacification occurred for PC samples starting at dose levels around 10^5 Gy for electron irradiation. Black materials maintained their color with no noticeable change, except for POM ELS, which seemed to lose its shiny appearance, turning its surface matt. PEEK samples showed a slight color shift towards warmer tones when irradiated with 10^6 Gy, regardless of particle type. Both PMMA and POM exhibited significant radiation induced stress fractures. While PMMA retained its structural integrity, POM samples were completely destroyed.

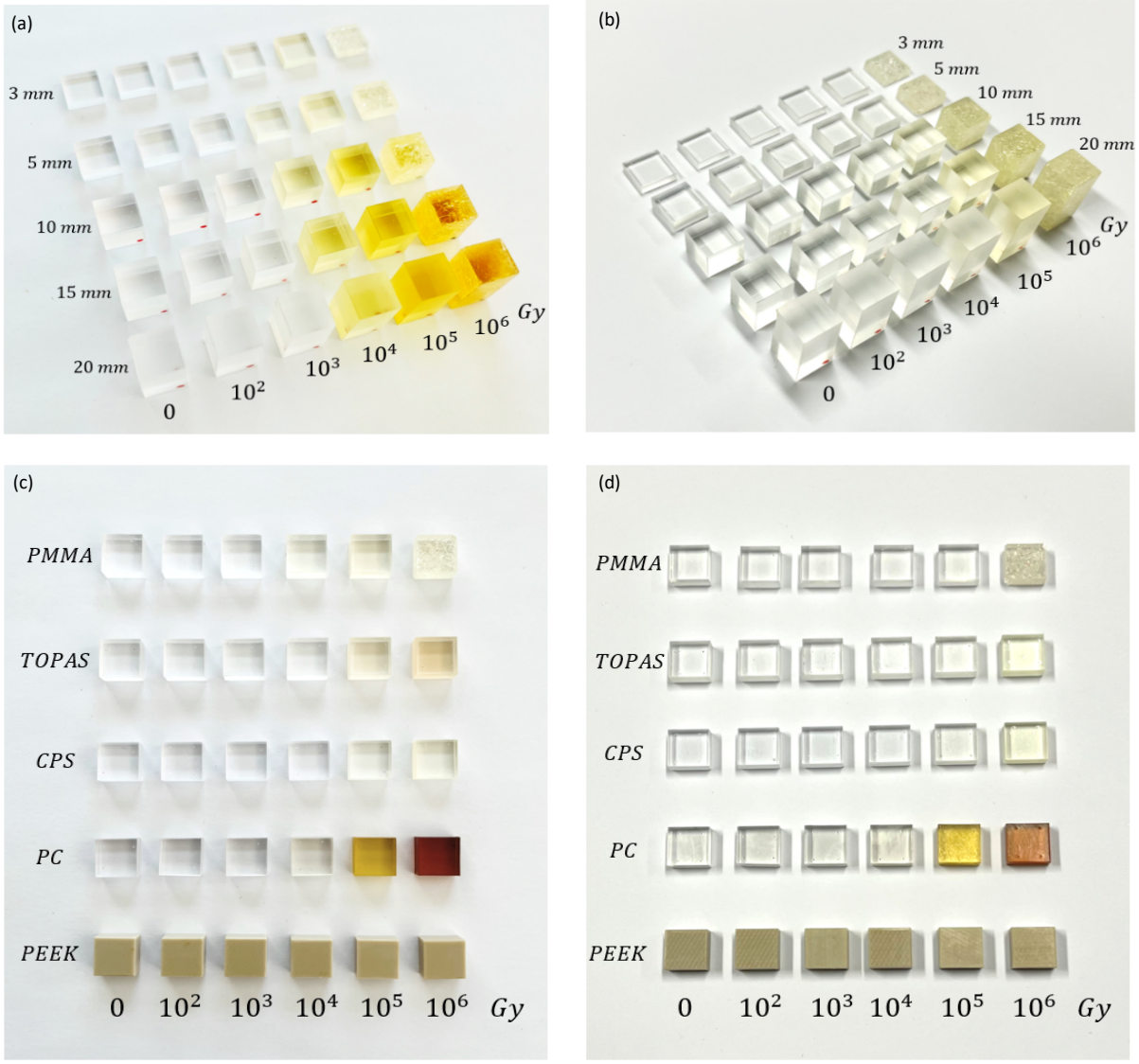

Figure 3: Type "E", electron irradiated samples in experiment SSD50. (a) PMMA samples of different thickness and dose levels. (b) Same samples as (a) two years later. (c) Different materials with 5 mm thickness and dose levels. (d) Same samples as (c) two years later.

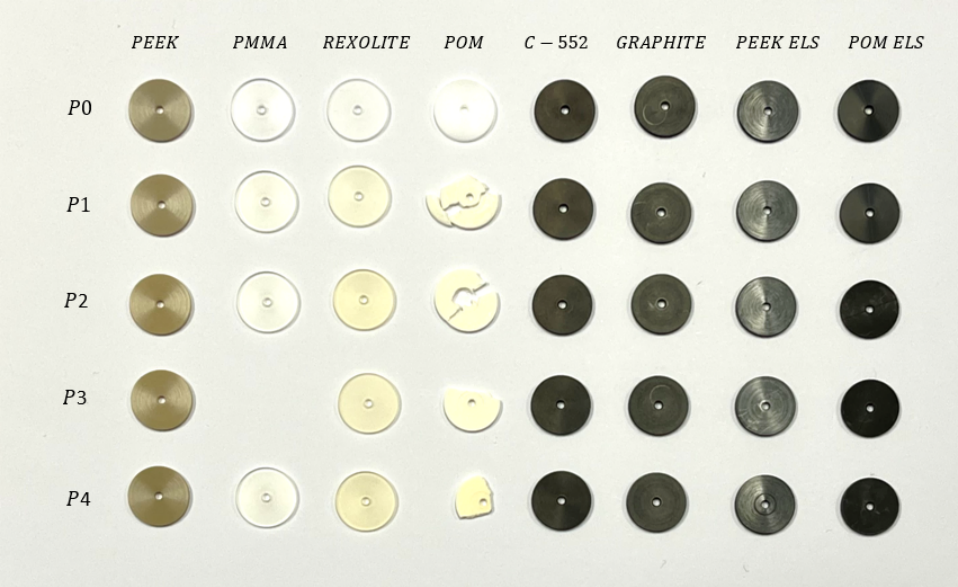

Figure 4: Type "P" samples; pristine (P0) and irradiated with proton beams under different conditions (P1 – P4).

3.1. Optical properties

UV-Vis analysis of PMMA indicated a decrease in transmittance spectra as the radiation dose increased (Figure 5(a)). This decrease correlates with the observed yellowing of the samples, likely attributed to the introduction of conjugated carbonyl groups in the polymer chain (Monsores et al., 2019). A partial recovery in color was observed two years post-irradiation, with UV-Vis analysis revealing up to a 30% increase in transmittance for thicker samples (>5 mm) and a 5–10% increase for thinner samples (≤5 mm).

Figure 5(b) highlights the dependence of transmittance on sample thickness for PMMA. Figures 5(c) and 5(d) show the transmittance at 420 nm for type "E" and "P" samples, respectively, for various materials. For PMMA type "E" samples, no significant differences in transmittance were observed between different dose rates (Figure 5(d)). Conversely, type "P" samples exhibited differences in transmittance; however, these differences did not show a clear correlation with dose rates.

When comparing the effects of different particle types, it is clear that no fair comparison can be made due to the dependence of the transmittance with the sample thickness. Figure 5(f) illustrates this dependency for type "E" and "P" PMMA samples irradiated with 1 MGy, showing a continuous trend across both sets.

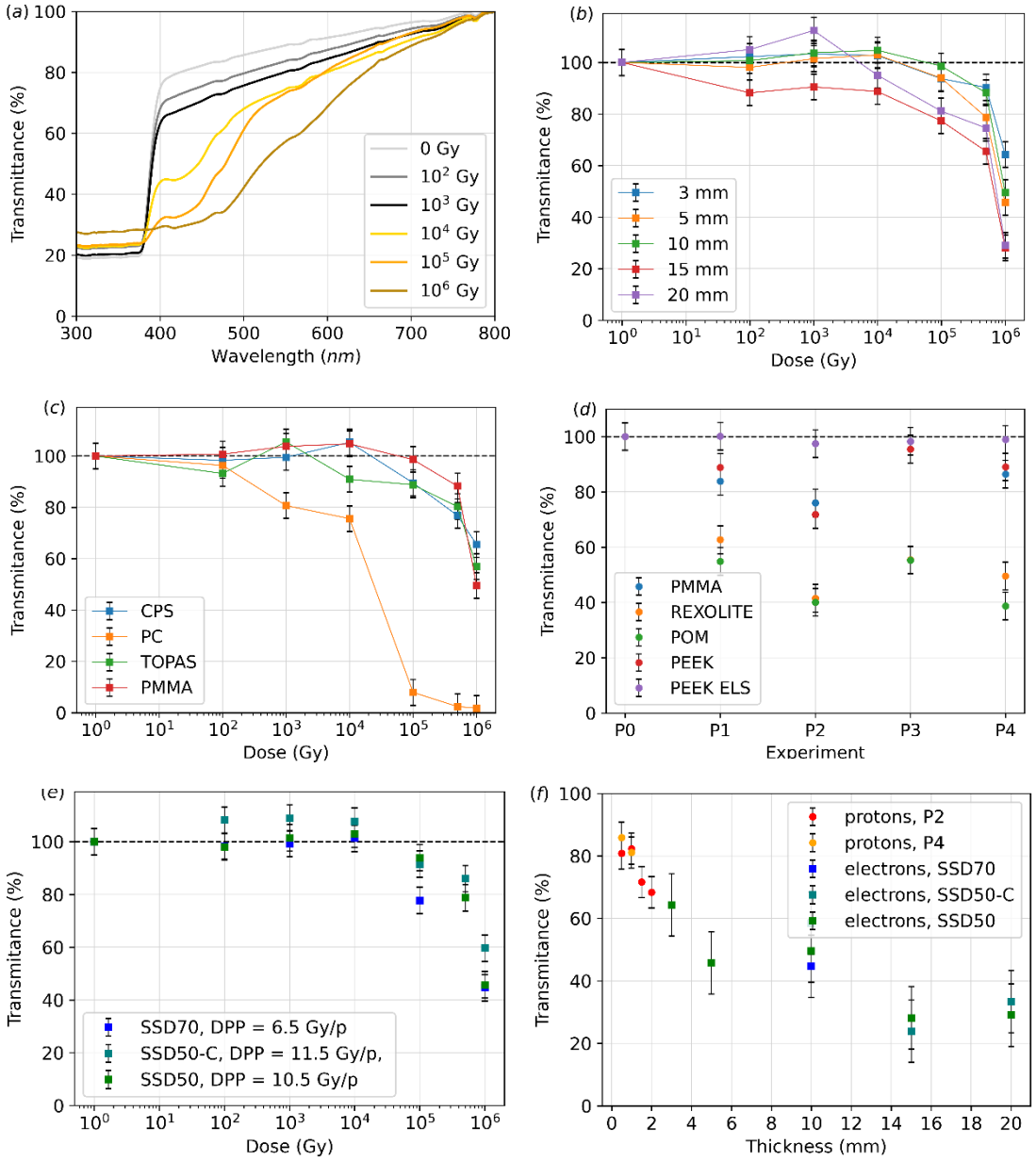

Figure 5: Results for the UV-Vis spectroscopy. (a) Example of the transmittance spectra for the different dose levels for the 2mm PMMA type "E", electron irradiated samples. (b) Transmittance of type "E" PMMA samples of different thicknesses irradiated with electrons in experiment SSD50 for different dose levels. (c) Transmittance comparison of type "E" different materials from experiment SSD50. (d) Transmittance comparison of type "P", proton irradiated materials for the 0.5mm samples. (e) Transmittance for different dose levels for type "E" PMMA samples irradiated at different dose rates. (f) Transmittance for different thickness of PMMA samples irradiated with 1MGy protons and electrons.

SEM analysis on conductive samples (Figure 6 (a)) revealed no observable differences in the surface of PEEK ELS and C-552 samples across the different irradiation conditions. For graphite samples, smoother and larger surface chunks were identified in irradiated sets compared to non-irradiated samples. These changes, did not exhibit significant variation between different experimental conditions, suggesting limited dependence on dose or dose rate.

Significant changes were found in the surface of POM ELS samples. Multiple rifts and surface fissures were evident, with the greatest density and size of rifts appearing in samples irradiated in experiment P2. This was followed by experiments P3 and P4, with progressively fewer rifts observed. However, no clear correlation was found between the observed changes and the dose rate.

Although SEM is not typically suitable for analyzing non-conductive samples, irradiated POM samples could be successfully analyzed, indicating an increase in surface conductivity induced by irradiation. This finding aligns with the electrical characterization results in Section 3.4. Figure 6(b) shows detailed SEM images of irradiated POM samples at different magnifications (x20, x200, x900, and x1600), highlighting the presence of rift-like patterns across the surface. These microstructures are consistent with the degradation seen in POM ELS samples and may be attributed to gas release during irradiation, as reported in previous studies (Elidrissi-Moubtassim et al., 2020). This phenomenon is likely caused by the formation and release of gaseous products, which leads to surface cracking.

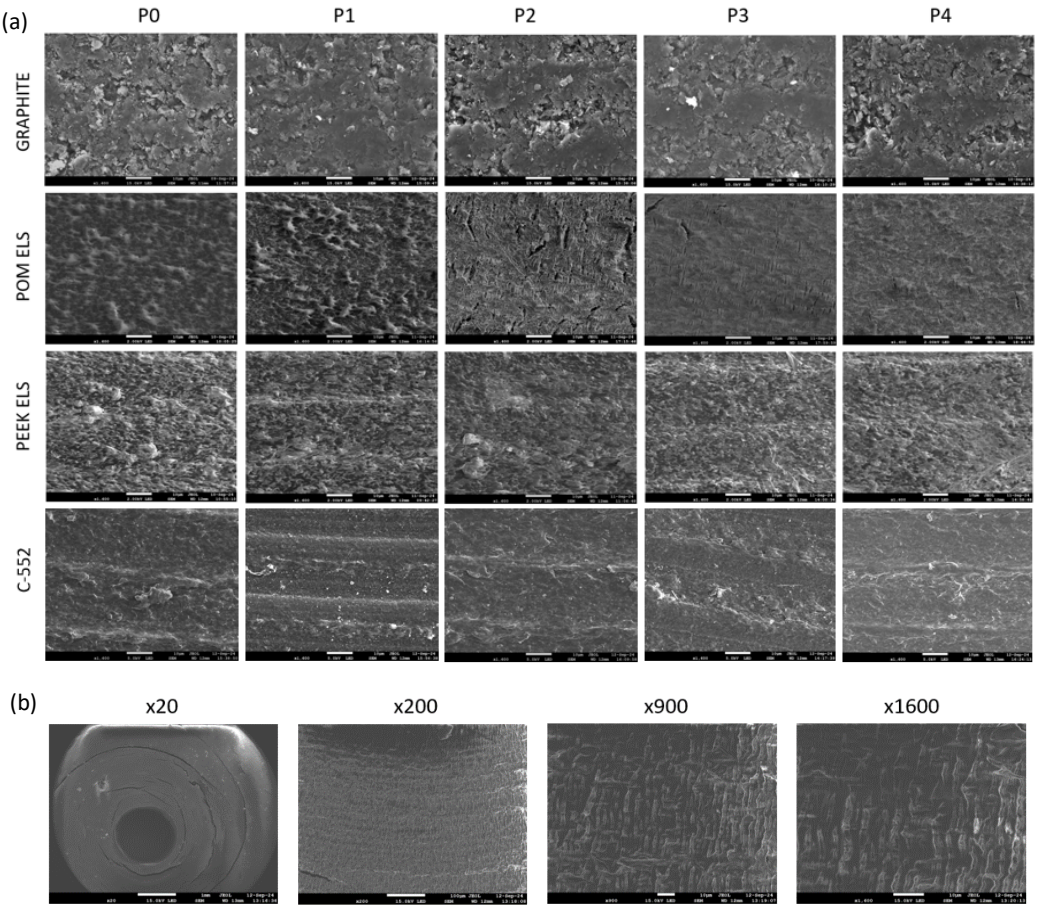

Figure 6: (a) SEM visualization of surface of 1mm type "P", proton irradiated samples, at x1600, accelerating voltage of 15kV from pristine samples (P0) and all consecutive experiments with protons (P1, P2, P3 & P4). (b) SEM visualization of surface of POM samples for different augmentations from experiment P4.

3.2. Chemical properties

The FTIR spectra of various materials are presented in Figures 7 – 10. This analysis focuses on the observed spectral changes, as a comprehensive discussion of all peaks is beyond this study's scope. Overall, the obtained spectra align well with their expected profiles.

FTIR analysis revealed no significant changes in the spectra of CPS, PEEK, REXOLITE and PEEK ELS spectra. For the remaining materials, FTIR analysis demonstrated that radiation-induced oxidative degradation, particularly the formation of carbonyl groups around 1720 cm^{-1}, was a common mechanism across all polymers (Celina et al., 2021). Specific spectral changes, varied depending on the material and dose level, with some evidence of partial recovery over time in certain cases. Specifically, C-552 showed a gradual, slight increase in absorbance around 1720 cm^{-1} and 2930 cm^{-1} with increasing dose levels, attributed to the formation of carbonyl groups and oxidation processes.

For PC electron irradiated samples, no changes were observed in the initial FTIR analysis (Y0). However, after two years (Y2), subtle modifications were detected, as shown in Figure 7, with slight peak shifts and changes in peak intensity with dose levels starting at 10^5 Gy. In the region 1330–1380 cm^{-1}, a gradual increase in absorbance was observed. The carbonyl group region (1700–1720 cm^{-1}) exhibited similar behavior, further confirming radiation-induced oxidative degradation (Gupta et al., 2015).

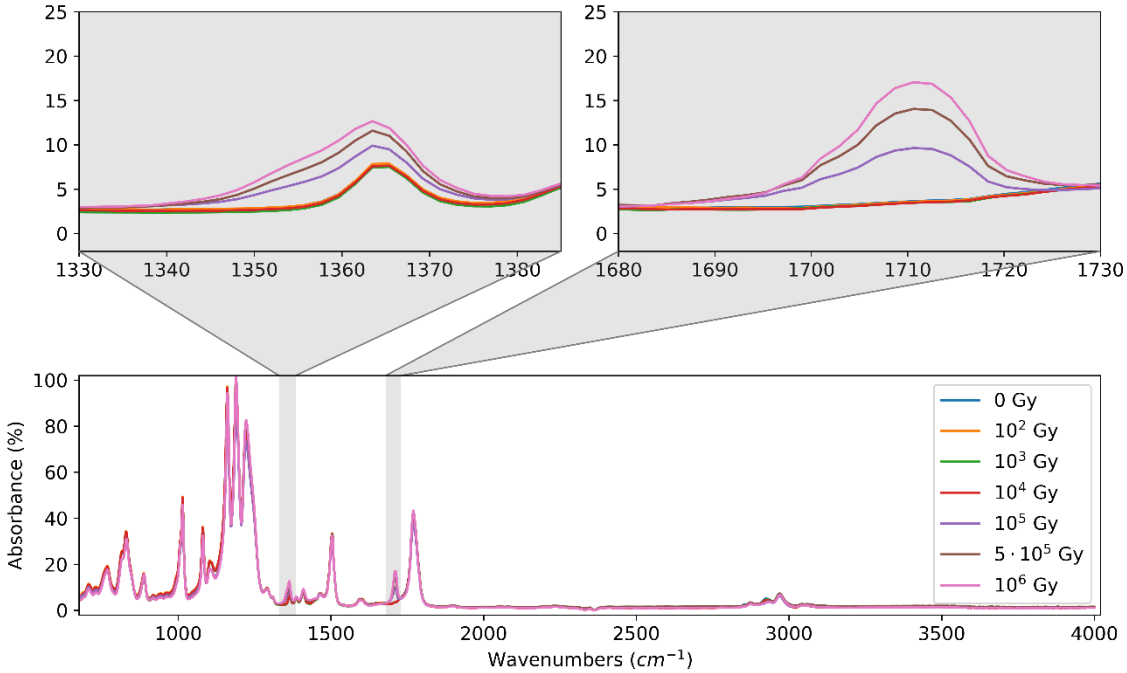

Figure 7: FTIR spectra of PC for different dose levels studied from experiment SSD50 of electron irradiated samples analyzed two years after the irradiation was performed.

TOPAS also showed dose-dependent changes, particularly an increase in absorbance around 1700 cm^{-1}, again associated with carbonyl group formation. In addition, a decrease in absorbance in the 2800–3000 cm^{-1} region was observed, reflecting possible C-H group modifications such as chain scission and cross-linking (Saunier et al., 2008). Analysis performed two years later revealed partial recovery, with a reduction in oxidation products in the carbonyl region (1500–1850 cm^{-1}) and an increase in absorbance in the C-H stretching region (2800–3050 cm^{-1}), indicating polymer chain reorganization and stabilization. Overall, while radiation damage was evident, some structural changes appeared to recover over time (see Figure 8).

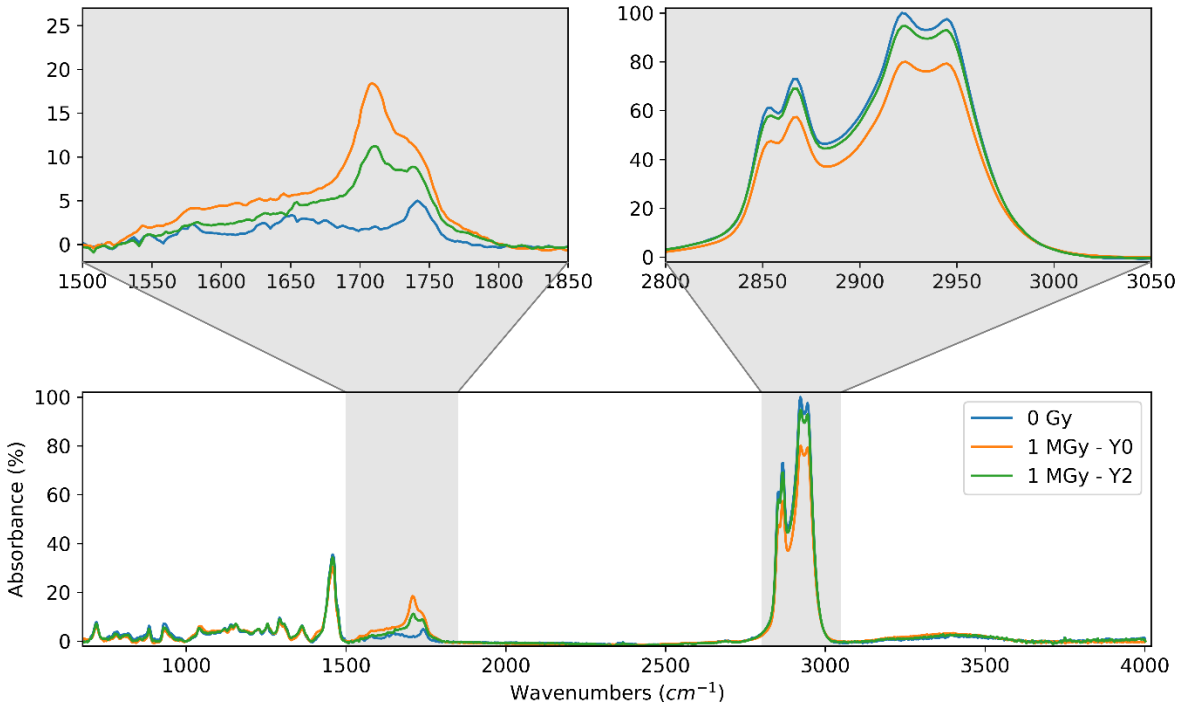

Figure 8: FTIR spectra of TOPAS irradiated with electrons. Comparison between non-irradiated sample (0Gy); Irradiated sample with 1MGy performed shortly after the experiment SSD50 (1 MGy - Y0); and the same 1MGy irradiated sample analyzed again two years later (1 MGy - Y2). Partial recovery is observed, as the Y2 spectrum tends to revert towards the shape of the non-irradiated spectrum.

POM exhibited a decrease in absorbance around 900 cm^{-1}, where characteristic C-O and C-H bonds appear. This decrease is attributed to oxidation and cross-linking, which disrupt these bonds. Additionally, an increase in absorbance in the 1700–1780 cm^{-1} region confirmed the presence of carbonyl groups from oxidative degradation (Ramirez et al., 2009). Among the experiments, the most significant differences were observed in P2, with progressively fewer changes in P3 and P4, and the smallest differences in P1, consistent with the lower radiation dose (see Figure 9 (a)).

Similarly, POM ELS showed a decrease in absorbance and peak broadening around 900 cm^{-1}, linked to oxidation and chain scission affecting C-O vibrational modes (Lim et al., 2022). The carbonyl region (1550–1750 cm^{-1}) exhibited an increase in absorbance, further confirming oxidative degradation. The progression of changes across different dose levels mirrored that observed in POM (Figure 9 (b)).

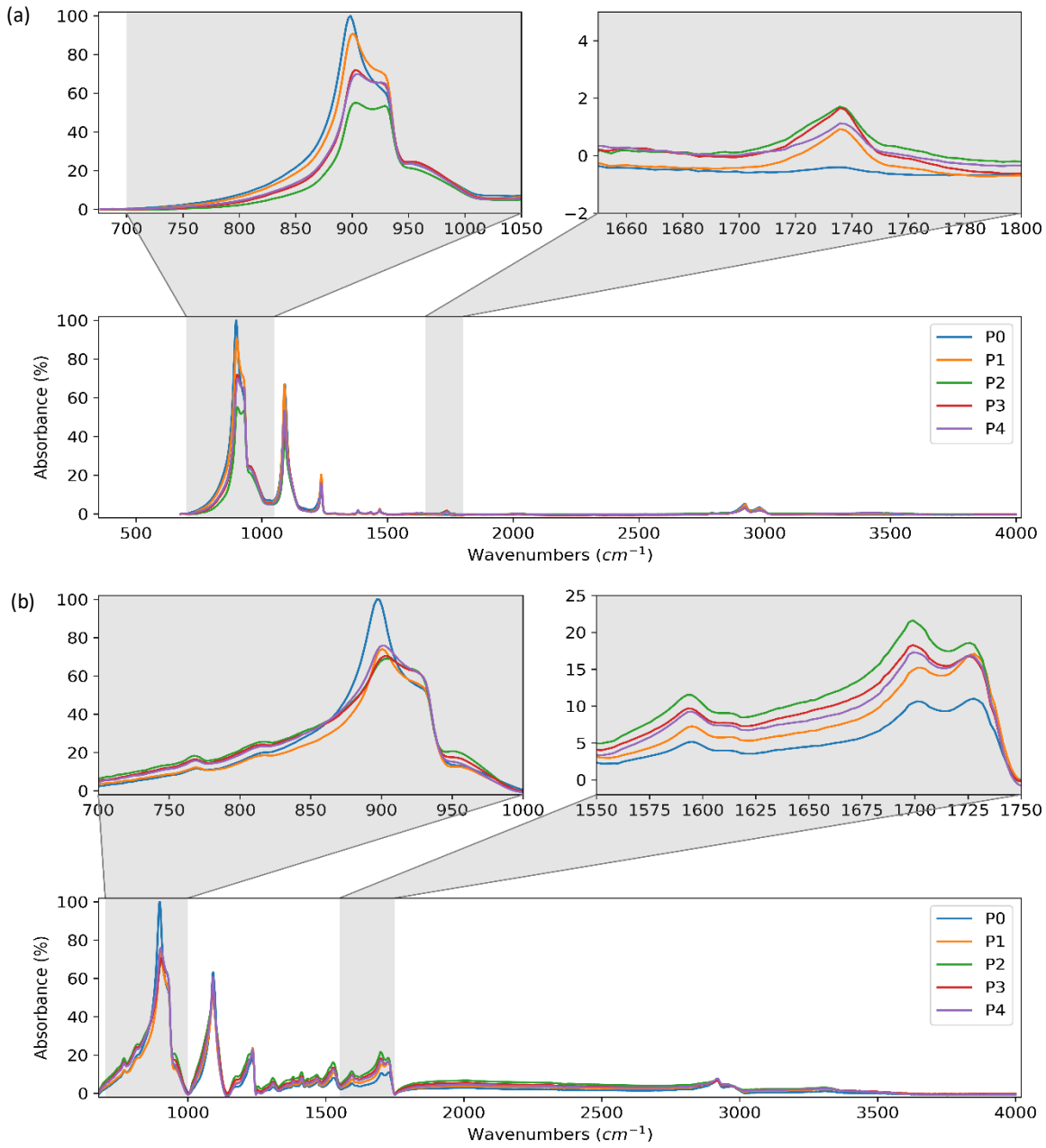

Figure 9: FTIR spectra of POM (a) and POM ELS (b) irradiated with protons.

PMMA showed some differences between the initial analysis (Y0) and the follow-up conducted two years later (Y2) as shown in Figure 10 (a), where the spectra highlight changes in both carbonyl (1720 cm^{-1}) and C-H regions (2800-3100 cm^{-1}) linked to oxidative degradation. A slight recovery of the material was observed. A comparison between electron and proton irradiation (Figure 10 (b)) revealed similar impact on the material, which was expected given the comparable LET of both particles under the investigated conditions (Monsores et al., 2019).

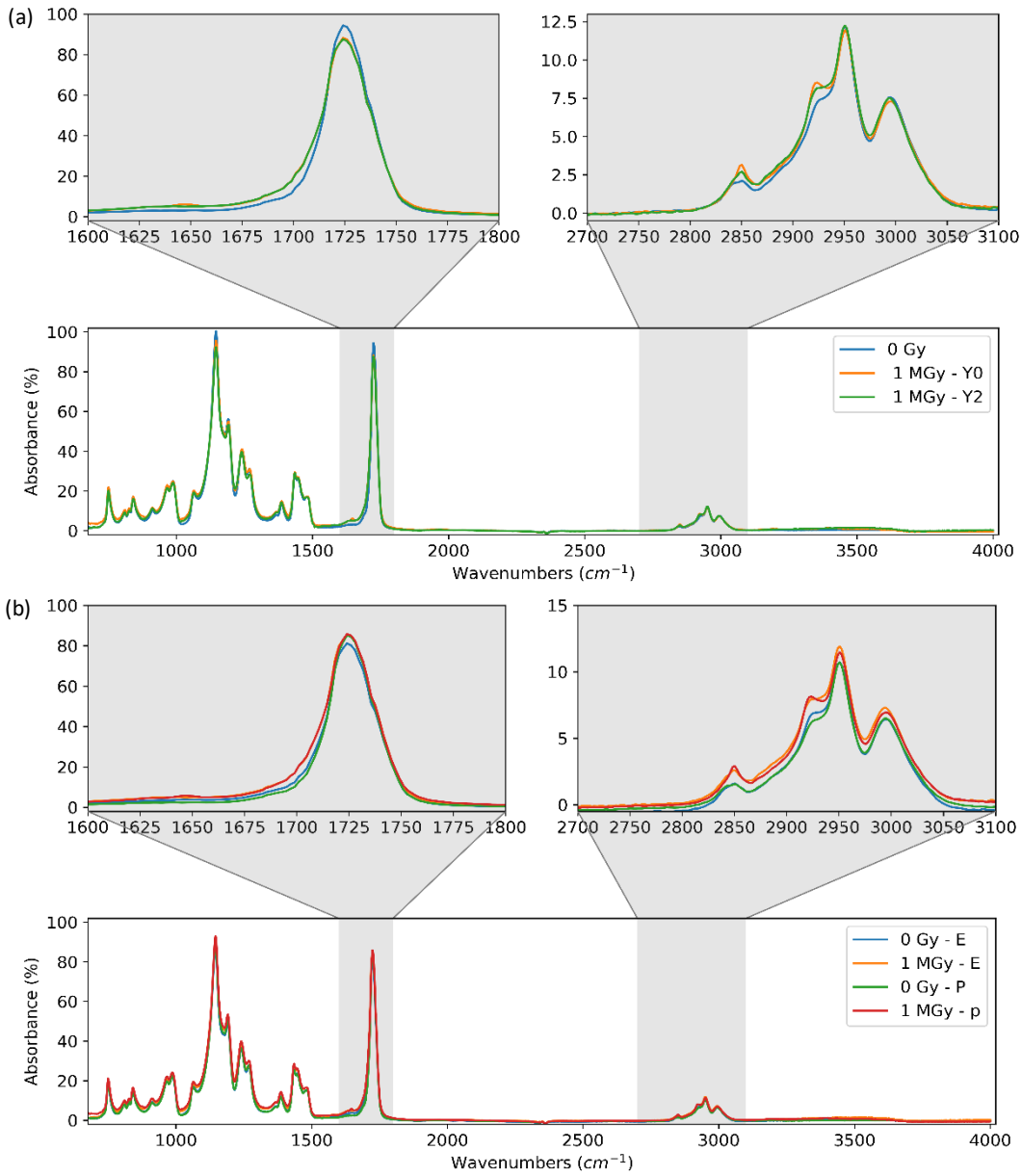

Figure 10: FTIR spectra of PMMA. (a) Comparison of electron irradiated samples between first FTIR (Y0) and secondary analysis performed two years later (Y2). (b) Comparison between electrons (SSD50 experiment) and protons (P2 experiment).

Representative Raman spectra of graphite samples irradiated with protons are presented on figure 11 (a) for the different conditions. The characteristic D band of graphite, observed around 1309 cm^{-1}, is associated with structural defects and disorder, while the G band around 1578 cm^{-1} corresponds to the stretching vibrations of sp^2 carbon-carbon bonds in the graphite lattice. Additionally, the D' band near 1605 cm^{-1} is related to further disorder in the graphitic structure. While the spectra are consistent with the expected vibrational modes of graphite (Chan et al., 2009), the irregular surface morphology of the

samples introduced significant statistical noise in the measurements. Despite this noise, no significant differences in the Raman spectra were identified across the experimental conditions.

Figure 11 (b) shows the intensity ratio between D and G bands, which offers information about possible structural disorder or defects. The Raman spectrum and ratio remained almost constant across all experimental conditions, with variations falling within the uncertainty range.

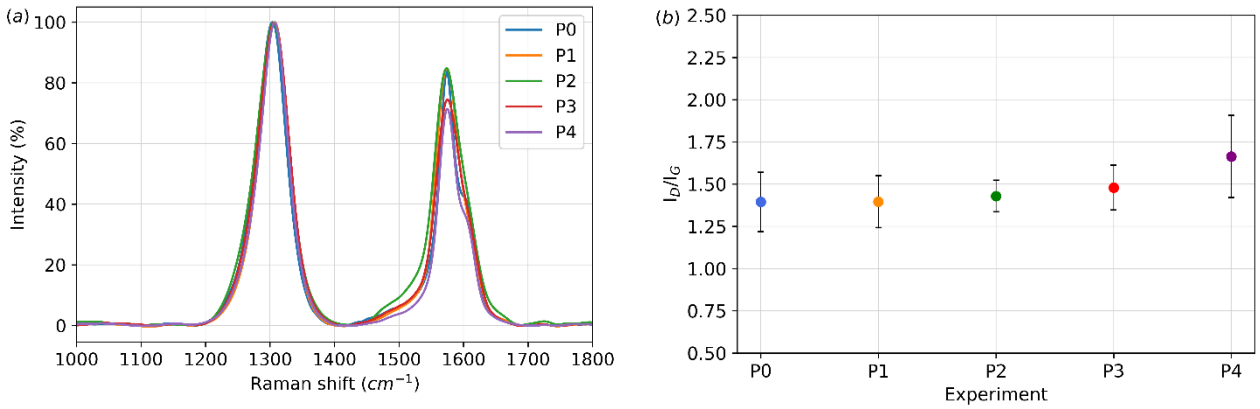

Figure 11: (a) Representative Raman spectra of graphite for the different experiments with protons. (b) Intensity ratio between D and G bands for different experiments.

3.3. Mechanical properties

Type "E" samples exhibited large manufacturing tolerances, and no measurable changes in dimensions were observed after irradiation. In contrast, Type "P" samples were fabricated with standard tolerances typically used for ICs construction (around $\pm$0.5%).

Figure 12 shows the relative changes in thickness and diameter averaged for the different materials and experimental conditions for type "P" samples. It can be clearly seen that POM and its conductive version, POM ELS exhibited significant dimensional reductions in both thickness and diameter.

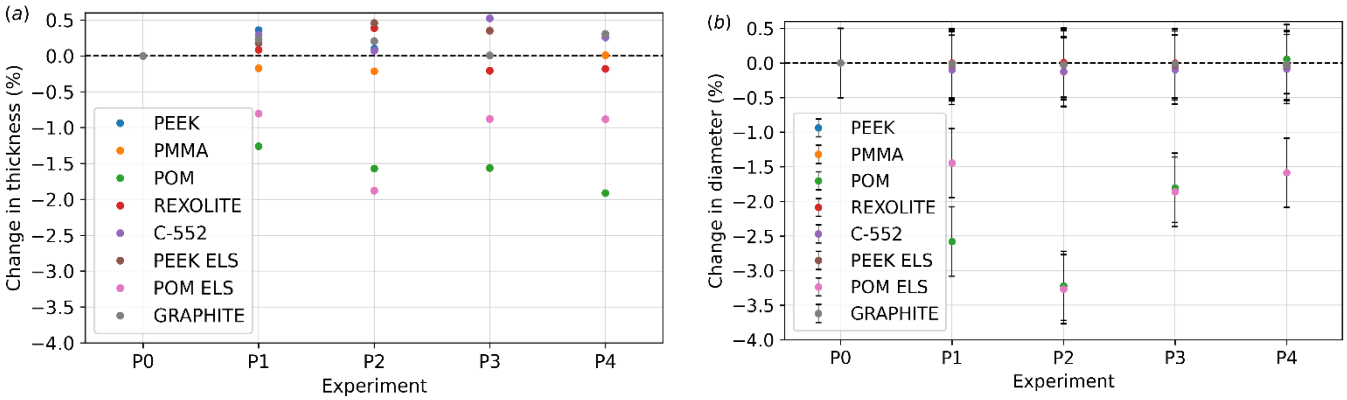

Figure 12: (a) Change in thickness for type "P", proton irradiated samples averaged for all thicknesses and normalized at the nominal value of the pristine samples. To enhance clarity no error bars were displayed. Typical type-A error was found around 0.5%. (b) Relative change in diameter.

Figure 13(a) presents the results of micro-indentation tests performed on Type “P” samples. POM irradiated samples fractured during testing, indicating significant material embrittlement. POM ELS showed a significant reduction in hardness, with similar results observed across experiments P2, P3, and P4, corresponding to approximate dose levels of 1 MGy. For Type “E” samples, the results are shown in Figure 13(b). PMMA demonstrated a significant decrease in hardness with increasing dose levels. The hardness of TOPAS exhibited only a slight reduction with dose, while other materials showed no significant changes. Figure 13(c) compares the hardness of PMMA Type “E” samples across different experiments and dose rates. The results indicate no measurable differences between the different dose rates. Furthermore, no change in hardness was observed when tests were repeated two years after irradiation (Y2) compared to the initial post-irradiation tests (Y0), suggesting that the reduction in hardness is permanent, with no recovery over time. Figure 13(d) provides a comparative analysis of PMMA Type “E” and Type “P” samples across different dose levels. Type “P” samples did not exhibit a decrease in hardness with dose levels, unlike Type “E” samples. This discrepancy may be attributed to substrate effects masking potential changes in the material.

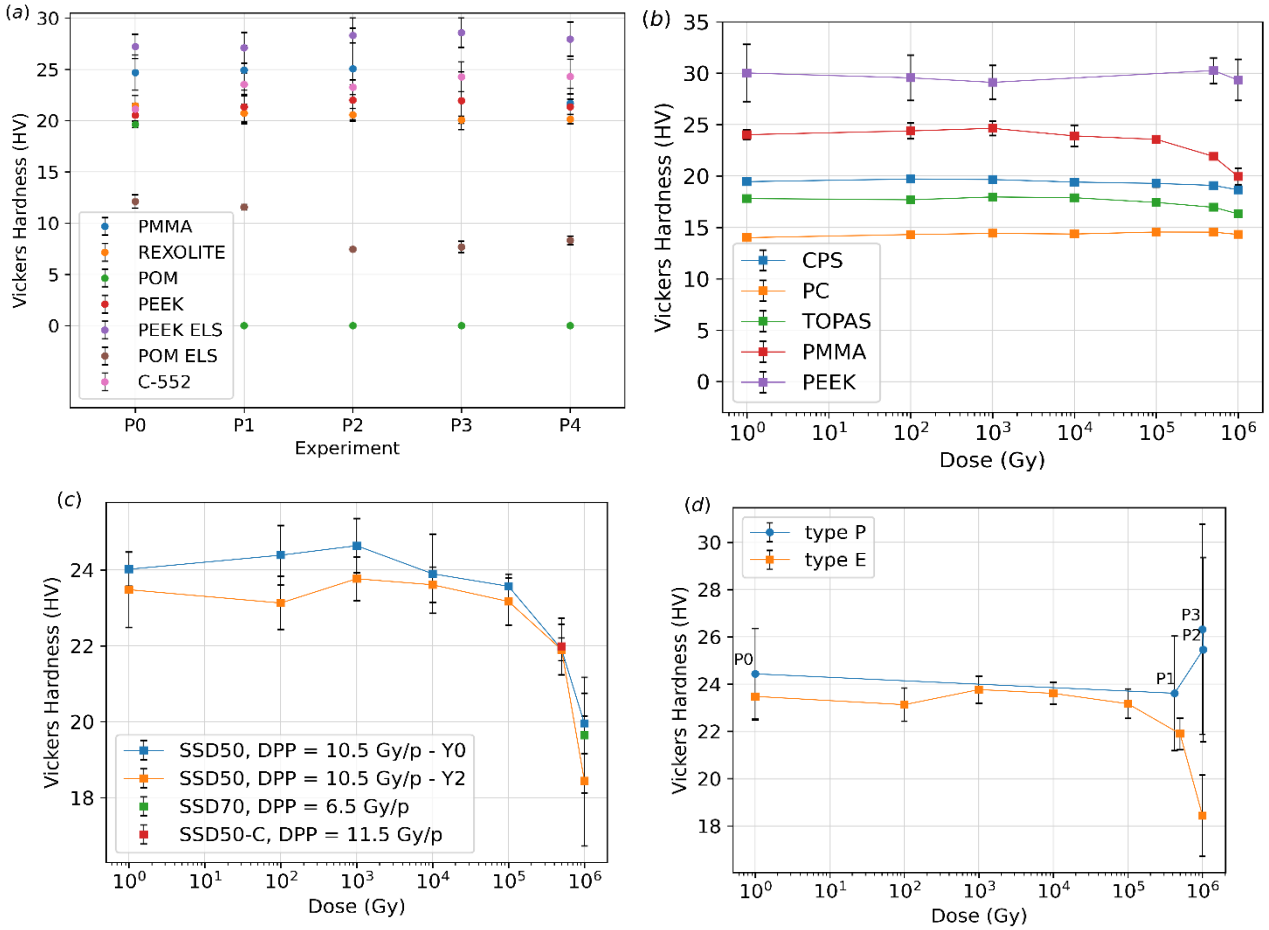

Figure 13: (a) Hardness tests results for the type “P” proton irradiated samples for different materials. (b) Hardness test for type “E” electron irradiated samples for different dose levels in experiment SSD50. (c) Hardness for type “E” PMMA samples for different dose rates. Results for SSD50 experiment are displayed for the analysis performed shortly after irradiation (Y0) and two years later (Y2). (d) Comparison of type “E” and “P” PMMA samples hardness.

During micro-indentation, formation of rifts around the indent were observed for some irradiated materials exposed to a dose of 1 MGy. Non-irradiated samples did not exhibit this rift formation, indicating an increase in sample fragility as a result of irradiation. This phenomenon was observed for PMMA (see figure 14), independently of the particle type, and in other materials such as PC, TOPAS, POM and POM ELS.

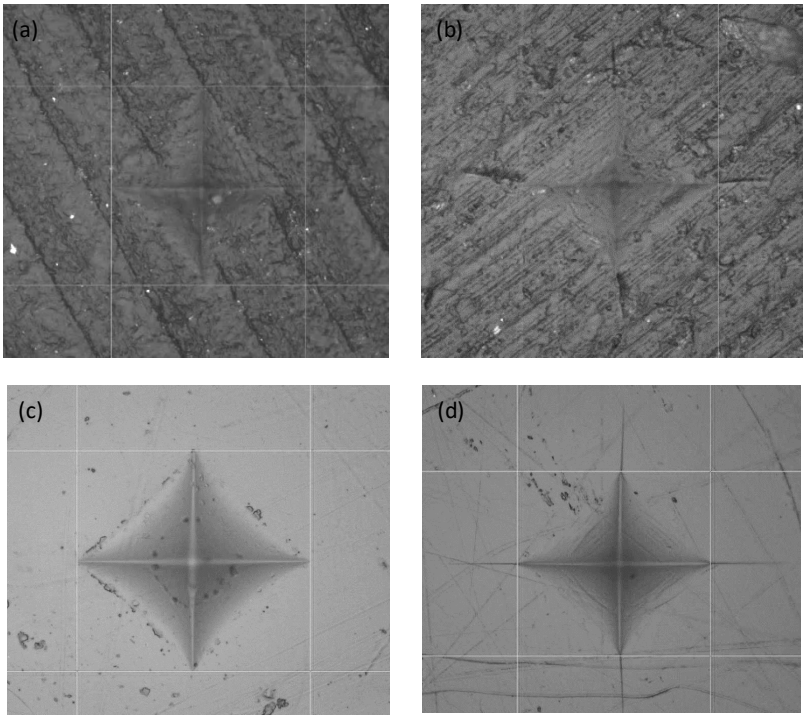

Figure 14: (a) 1mm PMMA indentation marks of non-irradiated type "P" samples. (b) Irradiated type "P", proton irradiated samples from experiment P4. (c) 3mm type "E" non-irradiated samples. (d) Electron irradiated type "E" samples with 1 MGy from experiment SSD50. It can be seen how the pressure from the indenter caused stress fractures around the diagonals, indicating a significant increase in fragility.

3.4. Electrical properties

Figure 15(a) presents the dielectric constant (ε) of type "E" PMMA samples irradiated at various dose levels as a function of frequency. Figure 15(b) illustrates the relative change in dielectric constant for various materials in type "E" samples. For samples of varying thickness, results were averaged across all thicknesses. No significant differences were observed across different dose levels, except in the case of PMMA, which exhibited a gradual increase in the dielectric constant of up to 7% starting at dose levels of 10^5 Gy. This increase was found to be independent of sample thickness.

Similarly, Figure 15(c) displays the relative change in dielectric constant for type "P" samples. Among these, only the dielectric constant of POM exhibited a notable change. Results for experiments P3 and P4 are not included due to the complete fragilization of samples during handling. Figure 15(d) highlights the dependence of the PMMA dielectric constant on sample thickness under different irradiation conditions. This observed variation in dielectric constant with thickness aligns with prior findings reported by (Gross et al., 2007)

As discussed in Section 3.1, a fair comparison between particle types cannot be made due to the intrinsic dependence of the dielectric constant on sample thickness. Nevertheless, a continuous trend is evident across both sets of samples. Furthermore, no change in the dielectric constant was observed in samples analyzed shortly after irradiation (Y0) or two years post-irradiation (Y2), indicating that the changes in this property did not vary over time.

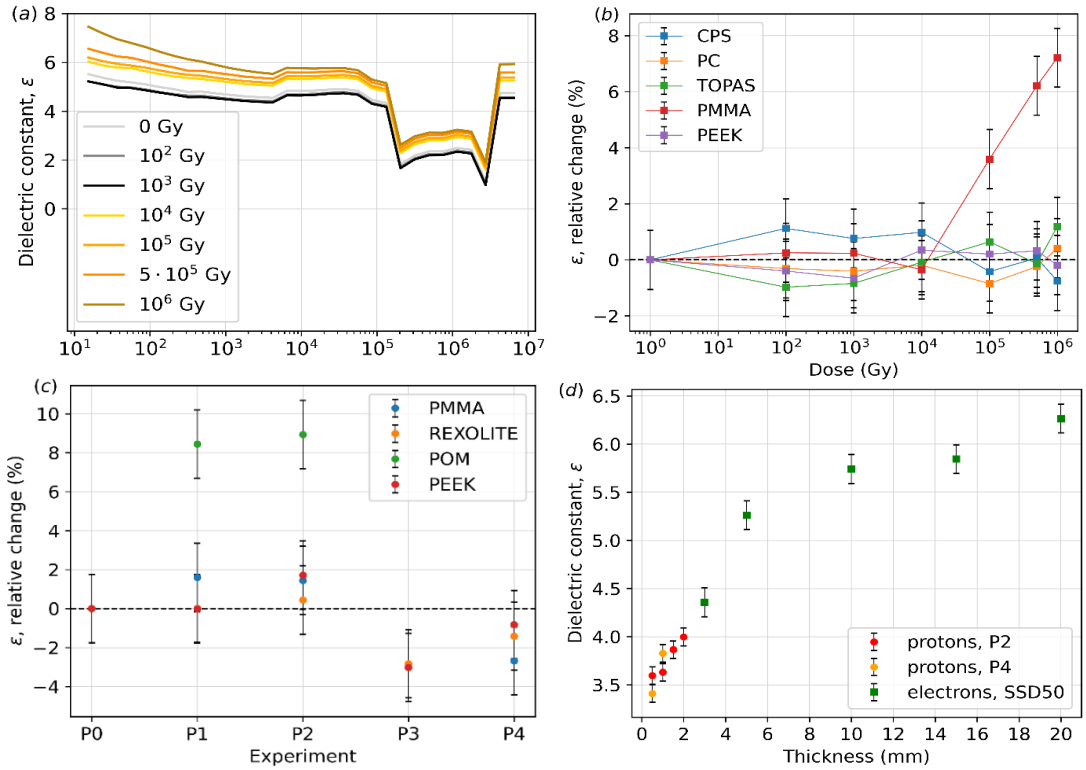

Figure 15: (a) Dielectric constant of PMMA for 1.5mm type "E", electron irradiated samples from experiment SSD50 as a function of frequency of the applied AC voltage signal. (b) Dielectric constant for type "E" samples and different dose levels from experiment SSD50. (c) Dielectric constant for type "P", proton irradiated samples. (d) Comparison of PMMA dielectric constant of protons and electrons.

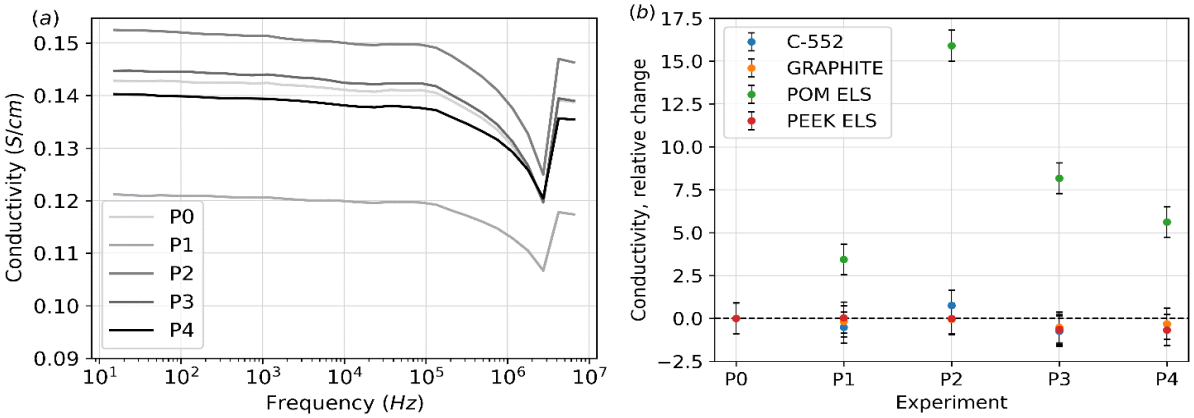

Figure 16: (a) Conductivity of graphite as a function of frequency of the applied AC voltage signal for different proton experiments (P). (b) Relative change of conductivity for the different samples and materials.

Figure 16 (a) presents graphite conductivity as a function of frequency. For relative comparison, conductivity values were taken at 1 MHz. Figure 16 (b) shows conductivity for various materials across different experiments with protons. It can be seen a significant change in conductivity for POM ELS samples. The largest relative change, compared to the non-irradiated condition (P0), was observed in experiment P2. Subsequent experiments, P3, P4, and P1, demonstrated progressively smaller relative changes. In contrast, the rest of materials did not exhibit any significant changes in conductivity.

4. Discussion

Table 4 provides an overview of the outcomes of the various tests conducted on different materials and sample types. The results indicate that radiation damage effects vary greatly depending on the material. In the following paragraphs, an overview of the most concerning changes in each of the materials is provided, clarifying what determines their suitability or not for ultra-high dose rate (UHDR) applications.

		Properties								
		Optical		Chemical		Mechanical			Electrical	
Material	Sample type	UV-VIS	SEM	FTIR	Raman	Dimensions	Hardness	*Fragility**	ε	Conductivity
PMMA	*E*	*x*	-	*x*	-	-	*x*	*x*	*x*	-
	P	*x*	-	*x*	-	*ok*	*ok*	*x*	*ok*	-
PEEK	*E*	-	-	*ok*	-	-	*ok*	*ok*	*ok*	-
	P	*ok*	-	*ok*	-	*ok*	*ok*	*ok*	*ok*	-
PC	*E*	*x*	-	*x*	-	-	*ok*	*x*	*ok*	-
TOPAS	*E*	~	-	*x*	-	-	~	*x*	*ok*	-
CPS	*E*	~	-	*ok*	-	-	*ok*	*ok*	*ok*	-
REXOLITE	*P*	~	-	*ok*	-	*ok*	*ok*	*ok*	*ok*	-
POM	*P*	*x*	-	*x*	-	*x*	*x*	*x*	*x*	-
C-552	*P*	-	*ok*	~	-	*ok*	~	*ok*	-	*ok*
GRAPHITE	*P*	-	~	-	*ok*	*ok*	-	*ok*	-	*ok*
POM ELS	*P*	-	*x*	*x*	-	*x*	*x*	*x*	-	*x*
PEEK ELS	*P*	*ok*	*ok*	*ok*	-	*ok*	*ok*	*ok*	-	*ok*

Table 4: Resume of the results of the different tests performed. "x" indicates crucial or very significant characteristics were altered in the sample. "ok" indicates no observable differences were found. "~" indicates small differences were found. "-" indicates test was not performed in that sample. Please note that Fragility was not measured directly, observed phenomena of cracks during Vickers indentation test provided information about material's brittleness.*

PMMA, POM, and its conductive variant (POM ELS) are strongly discouraged for use in UHDR conditions due to significant degradation found in most properties, specially brittleness that compromised its structural integrity. This issue is evident in the ICs and the top-right water phantom images from Figure 1, all made of PMMA (note that the bottom-left IC is covered by a thin layer of black lacquer). PC is also not recommended; although most of its properties remained invariant, the loss of transparency makes it impractical for see-through applications. Evidence of this issue can be seen in the water phantom in the bottom-right image of Figure 1. TOPAS demonstrated only a slight increase in fragility, but substantial changes in its chemical properties raise concerns about its long-term performance, especially under higher doses that exceed the range of this study. Materials such as Rexolite and C-552 proved to be completely functional even though subtle changes in some properties were observed.

The following materials showed the most resistance to radiation and are therefore recommended to use for UHDR applications: CPS, PEEK, Graphite and PEEK ELS. CPS, which is highly recommended for see

through applications, as its properties remained unchanged except for slight coloration around dose levels of 1 MGy. It represents a more durable alternative to PMMA, which is currently widely used for such purposes. For non-conductive, non-transparent applications, PEEK proved to be the most durable option, with only minor discoloration observed. For further evidence, the electron experiment holder was made entirely of PEEK, withstanding cumulative doses exceeding 25 MGy without visible damage, as supported by (Tavlet et al., 1998). For conductive applications, graphite remained a durable choice, as no significant changes in chemical, mechanical or conductive properties were observed. While minor surface changes were observed in SEM analysis, these could not be correlated with dose levels or dose rates. Though less conductive, PEEK ELS is also a viable alternative to graphite for conductive applications as all properties remained completely unaffected.

Several additional observations regarding material behavior under UHDR conditions were made in this study due to the variety of conditions tested. Test repeated two years after irradiation revealed recovery effects (Clough et al., 1995) in the optical and chemical properties of some materials, suggesting that for less exhaustive use, materials irradiated at similar doses as in this study may have extended lifespans in real applications. Chemical analysis of PMMA samples indicated that the type of particle used during irradiation did not influence material degradation; similar dose levels resulted in comparable radiation damage, which is consistent with findings reported in the literature (Ferry et al., 2016).

Regarding dose rate effects, type “E” samples irradiated with electrons showed no significant difference in damage when comparing the different dose rates explored, suggesting that UHDR does not inherently produce more damage. Instead, UHDR enables higher total doses to be achieved more efficiently. However, under conventional use, healing effects may contribute to enhanced material durability over time.

Experiments with protons consistently showed that the highest damage in the materials occurred in experiment P2, followed by P3, P4, and P1. This order did not correlate with either instantaneous or average dose rates but rather with longer irradiation times. These findings suggest that heat damage contributed to the radiation damage, which may explain the observed results. Supporting this explanation, type “P” samples were irradiated in air, while type “E” samples were irradiated in water, which dissipated heat more effectively and protected them from heat damage.

Notably, the temperature increase due to radiation varies depending on the heat capacity of different materials, with graphite experiencing approximately 1.4 mK/Gy (Sakama et al., 2008). While specific values for the temperature rise due to radiation in PMMA and PEEK are not available, their similar heat capacities –approximately 1.09 J/g·K (Cheng et al., 1987; Rivière et al., 2016) for PEEK and 1.12 J/g·K (National Institute of Standards and Technology (NIST), n.d.; Pavlinov et al., 1967) for PMMA– suggest comparable temperature increase due to radiation. The difference in damage observed between PMMA and PEEK, despite their similar heat capacities, highlights that the resistance of polymers depends mainly on their chemical structure. The most resistant materials (CPS, PEEK, Graphite and PEEK ELS) have in common aromatic rings in their composition, that enhances their resistance to radiation (Ferry et al., 2012).

Notably, in this study, the total dose significantly surpasses the integrated doses that different dosimetry devices typically receive over their lifetime. However, due to the challenges in UHDR dosimetry, extensive studies are required to properly characterize UHDR beams. Furthermore, for clinical translation, certain measurements will require prolonged irradiation times—for instance, relative dosimetry, where

percentage depth dose curves or field size measurements with ionization chambers are necessary for commissioning—making the accumulation of high doses in QA devices at UHDR unavoidable in practice.

5. Conclusions

The findings of this study emphasize the complexity of radiation damage mechanisms and the importance of evaluating material properties and irradiation conditions when selecting materials for UHDR applications. The still-developing state of UHDR dosimetry and the need of exhaustive beam characterization for clinical translation of FLASH therapy make UHDR inherently associated with high radiation doses to QA devices in practice.

It has been observed that materials with aromatic rings in their chemical structure exhibit the highest stability under radiation, as demonstrated by the most resistant materials in this study. Depending on the application, different materials are recommended: CPS for transparent applications, PEEK for non-transparent and non-conductive applications, graphite for conductive applications, and PEEK ELS for lower-conductivity applications. As previously noted by (Ivanov & Koroleva, 1998), a polymer's resistance under ionizing radiation can be predicted if its macromolecular structure is well understood.

Acknowledgements:

The authors would like to thank Olaf Tappe for manufacturing the sample and providing the equipment for the measurement setup in the electron beam. Grateful acknowledgment is also extended to Christoph Makowski for his assistance in operating the electron accelerator and to Jose Paz Martin for kindly providing one of the IC images in Figure 1, which effectively illustrates the motivation of this work. The authors further acknowledge Sabine Bebelman, François Devred, Sophie Ryelandt, and Pascal Simon for the technical training sessions on the different equipment at UCLouvain, which enabled the exhaustive characterization of the samples.

This work has been partially funded by the Walloon Region under the project name D-CAF (Dosimetry for Carbon, ARC, and FLASH therapies), MecaTech/BioWin convention #8510; and by the EMPIR project 18HLT04 UHDpulse which has received funding from the EMPIR programme co-financed by the Participating States and from the European Union's Horizon 2020 research and innovation programme.

Bibliography:

Almond, P., Biggs, P., Coursey, B., Hanson, W., Huq, M., Nath, R., & Rogers, D. (1999). AAPM's TG-51 protocol for clinical reference dosimetry of high-energy photon and electron beams. In *Medical Physics (Lancaster)*. https://doi.org/10.1118/1.598691

Andreo, P., Burns, D. T., Hohlfeld, K., Kanai, T., Laitano, F., & Smyth, V. (2024). *Absorbed Dose Determination in External Beam Radiotherapy: An International Code of Practice for Dosimetry based on Standards of Absorbed Dose to Water*.

Bourgouin, A., Hackel, T., Marinelli, M., Kranzer, R., Schüller, A., & Kapsch, R. (2022). Absorbed-dose-to-water measurement using alanine in ultra-high-pulse-dose-rate electron beams. *Physics in Medicine and Biology*. https://doi.org/10.1088/1361-6560/ac950b

Bourgouin, A., Knyziak, A., Marinelli, M., Kranzer, R., Schüller, A., & Kapsch, R. (2022). Characterization of the PTB ultra-high pulse dose rate reference electron beam. *Physics in Medicine and Biology*. https://doi.org/10.1088/1361-6560/ac5de8

Celina, M., Linde, E., & Martinez, E. (2021). Carbonyl Identification and Quantification Uncertainties for Oxidative Polymer Degradation. *Polymer Degradation and Stability*. https://doi.org/10.1016/j.polymdegradstab.2021.109550

Chan, T., Dvoynenko, M., Liu, C., Wang, J.-K., & Wang, Y. (2009). Tip-enhanced Raman spectroscopy of graphite irradiated by focused ion beam. *Optics Letters*. https://doi.org/10.1364/ol.34.002246

Cheng, S. Z. D., Lim, S., Judovits, L. H., & Wunderlich, B. (1987). Heat capacities of high melting polymers containing phenylene groups. *Polymer*. https://doi.org/10.1016/0032-3861(87)90313-2

Christensen, J. B., Almhagen, E., Stolarczyk, L., Liszka, M., Hernandez, G. G., Bassler, N., Nørrevang, O., & Vestergaard, A. (2020). Mapping initial and general recombination in scanning proton pencil beams. *Physics in Medicine and Biology*, *65*(11). https://doi.org/10.1088/1361-6560/ab8579

Clough, R. L., Malone, G. M., Gillen, K. T., Wallace, J. S., & Sinclair, M. B. (1995). Discoloration and subsequent recovery of optical polymers exposed to ionizing radiation. *Polymer Degradation and Stability*. https://doi.org/10.1016/0141-3910(95)87013-x

Diffenderfer, E. S., Verginadis, I. I., Kim, M. M., Shoniyozov, K., Velalopoulou, A., Goia, D., Putt, M. E., Hagan, S., Avery, S., Teo, K., Zou, W., Lin, A., Swisher-McClure, S., Koch, C. J., Kennedy, A. R., Minn, A. J., Maity, A., Busch, T. M., Dong, L., … Cengel, K. A. (2020). Design, Implementation, and in Vivo Validation of a Novel Proton FLASH Radiation Therapy System. *International Journal of Radiation Oncology, Biology, Physics*. https://doi.org/10.1016/j.ijrobp.2019.10.049

Favaudon, V., Caplier, L., Monceau, V., Pouzoulet, F., Sayarath, M., Fouillade, C., Poupon, M., Brito, I., Hupé, P., Bourhis, J., Hall, J., Fontaine, J., & Vozenin, M. (2014). Ultrahigh dose-rate FLASH irradiation increases the differential response between normal and tumor tissue in mice. *Science Translational Medicine*. https://doi.org/10.1126/scitranslmed.3008973

Ferry, M., Bessy, E., Harris, H., Lutz, P., Ramillon, J., Ngono-ravache, Y., & Balanzat, E. (2012). Irradiation of ethylene/styrene copolymers: evidence of sensitization of the aromatic moiety as counterpart of the radiation protection effect. *The Journal of Physical Chemistry. B*. https://doi.org/10.1021/jp209535p

Ferry, M., Ngono-Ravache, Y., Aymes-Chodur, C., Clochard, M. C., Coqueret, X., Cortella, L., Pellizzi, E., Rouif, S., & Esnouf, S. (2016). Ionizing Radiation Effects in Polymers. *Reference Module in Materials Science and Materials Engineering*. https://doi.org/10.1016/B978-0-12-803581-8.02095-6

Friedel, R. A., & Carlson, G. L. (1971). Infrared spectra of ground graphite. *The Journal of Physical Chemistry*. https://doi.org/10.1021/j100678a021

Gross, S., Camozzo, D., Noto, V. Di, Armelao, L., & Tondello, E. (2007). PMMA: A key macromolecular component for dielectric low-κ hybrid inorganic–organic polymer films. *European Polymer Journal*. https://doi.org/10.1016/j.eurpolymj.2006.12.012

Gupta, D., Kumar, S., Kalsi, P. C., Manchanda, V., & Mittal, V. (2015). *γ-Ray Modifications of Optical/Chemical Properties of Polycarbonate Polymer*. https://doi.org/10.4236/wjcmp.2015.53015

Ivanov, V. V, & Koroleva, E. B. (1998). Radiation Resistance of Polymers and Polymer Materials. In V. V Ivanov (Ed.), *Radiation Resistance of Polymers* (pp. 89–112). CRC Press. https://doi.org/10.1201/9780429071003-5

Kranzer, R., Schüller, A., Bourgouin, A., Hackel, T., Poppinga, D., Lapp, M., Looe, H., & Poppe, B. (2022). Response of diamond detectors in ultra-high dose-per-pulse electron beams for dosimetry at FLASH radiotherapy. *Physics in Medicine and Biology*. https://doi.org/10.1088/1361-6560/ac594e

Lim, K., Hayat, M. Q., Jena, K. D., Zhang, W., Cao, P., Lim, K., Hayat, M. Q., Jena, K. D., Zhang, W., & Cao, P. (2022). On amine treated polyoxymethylene (POM) blends with low formaldehyde emission for metal injection moulding (MIM). *Journal of Materials Science*. https://doi.org/10.1007/s10853-022-07586-x

Martino, F. di, Barca, P., Barone, S., Bortoli, E., Borgheresi, R., Stefano, S. De, Francesco, M. Di, Grasso, L., Linsalata, S., Marfisi, D., Pacitti, M., & Felici, G. (2020). FLASH Radiotherapy With Electrons: Issues Related to the Production, Monitoring, and Dosimetric Characterization of the Beam. *Frontiers of Physics*. https://doi.org/10.3389/fphy.2020.570697

Monsores, K. G. de C., Silva, A. O. da, Oliveira, S. de S. A., Rodrigues, J. G. P., & Weber, R. P. (2019). Influence of ultraviolet radiation on polymethylmethacrylate (PMMA). *Journal of Materials Research and Technology*. https://doi.org/10.1016/j.jmrt.2019.06.023

Montay-Gruel, P., Acharya, M. M., Petersson, K., Alikhani, L., Yakkala, C., Allen, B. D., Ollivier, J., Petit, B., Jorge, P. G., Syage, A. R., Nguyen, T., Baddour, A. A. D., Lu, C., Singh, P., Moeckli, R., Bochud, F., Germond, J. F., Froidevaux, P., Bailat, C., … Limoli, C. L. (2019). Long-term neurocognitive benefits of FLASH radiotherapy driven by reduced reactive oxygen species. *Proceedings of the National Academy of Sciences of the United States of America*. https://doi.org/10.1073/pnas.1901777116

National Institute of Standards and Technology (NIST). (n.d.). *Poly(methyl methacrylate) (PMMA) - Thermophysical Properties*. Retrieved February 18, 2025, from https://webbook.nist.gov/cgi/cbook.cgi?ID=C87210320&Units=SI&Mask=2

Pavlinov, L. I., Rabinovich, I. B., Okladnov, N. A., & Arzhakov, S. A. (1967). *Heat capacity of copolymers of methyl methacrylate with methacrylic acid in the region 25–190°C*. https://doi.org/10.1016/0032-3950(67)90072-x

Poirier, F., Blain, G., Bulteau-harel, F., Fattahi, M., Goiziou, X., Haddad, F., Koumeir, C., Letaeron, A., & Vandenborre, J. (2019). *The Pulsing Chopper-Based System of the Arronax C70XP Cyclotron*. https://doi.org/10.18429/jacow-ipac2019-tupts008

Ramirez, N. V., Sánchez-Soto, M., Illescas, S., & Gordillo, A. (2009). *Thermal Degradation of Polyoxymethylene Evaluated with FTIR and Spectrophotometry*. https://doi.org/10.1080/03602550902725472

Rivière, L., Caussé, N., Lonjon, A., Dantras, E., & Lacabanne, C. (2016). Specific heat capacity and thermal conductivity of PEEK/Ag nanoparticles composites determined by Modulated-Temperature

Differential Scanning Calorimetry. *Polymer Degradation and Stability*. https://doi.org/10.1016/j.polymdegradstab.2015.11.015

Rossomme, S., Horn, J., Brons, S., Jäkel, O., Mairani, A., Ciocca, M., Floquet, V., Romano, F., Rodriguez Garcia, D., Vynckier, S., & Palmans, H. (2017). Ion recombination correction factor in scanned light-ion beams for absolute dose measurement using plane-parallel ionisation chambers. *Physics in Medicine and Biology*, *62*(13), 5365–5382. https://doi.org/10.1088/1361-6560/aa730f

Sakama, M., Kanai, T., & Fukumura, A. (2008). Development of a portable graphite calorimeter for radiation dosimetry. *Igaku Butsuri : Nihon Igaku Butsuri Gakkai Kikanshi = Japanese Journal of Medical Physics : An Official Journal of Japan Society of Medical Physics*. https://doi.org/10.11323/jjmp2000.28.1_1

Saunier, J., Chodur, C. A., Leclerc, B., Larbes, L., & Yagoubi, N. (2008). *Using COC as pharmaceutical or cosmetic storage material. II. Effect of electron beam radio-sterilization*. https://doi.org/10.1002/app.28275

Subiel, A., Bourgouin, A., Kranzer, R., Peier, P., Frei, F., Gómez, F., Knyziak, A., Fleta, C., Bailat, C. J., & Schüller, A. (2024). Metrology for advanced radiotherapy using particle beams with ultra-high dose rates. *Physics in Medicine and Biology*. https://doi.org/10.1088/1361-6560/ad539d

Subiel, A., & Romano, F. (2023). Recent developments in absolute dosimetry for FLASH radiotherapy. *British Journal of Radiology*. https://doi.org/10.1259/bjr.20220560

Tavlet, M., Schönbacher, H., & Fontaine, A. (1998). *Compilation of radiation damage test data*. https://doi.org/10.5170/cern-1998-001

Villoing, D., Koumeir, C., Bongrand, A., Guertin, A., Haddad, F., Métivier, V., Poirier, F., Potiron, V., Servagent, N., Supiot, S., Delpon, G., & Chiavassa, S. (2022). Proton beam dosimetry at ultra-high dose rates (FLASH): evaluation of GAFchromic™ (EBT3, EBT-XD) and OrthoChromic (OC-1) film performances. *Medical Physics (Lancaster)*. https://doi.org/10.1002/mp.15526

Zhou, S., Zheng, D., Fan, Q., Yan, Y., Wang, S., Lei, Y., Besemer, A. E., Zhou, C., & Enke, C. A. (2020). Minimum dose rate estimation for pulsed FLASH radiotherapy: A dimensional analysis. *Medical Physics (Lancaster)*. https://doi.org/10.1002/mp.14181